Rethinking Detecting Salient and Camouflaged Objects in Unconstrained Scenes

Zhangjun Zhou 1* Yiping Li 1* Chunlin Zhong 1* Jianuo Huang 1 Jialun Pei 2 Hua Li 3 He Tang 1†

¹Huazhong University of Science and Technology ²The Chinese University of Hong Kong, ³Hainan University

Abstract

While the human visual system employs distinct mechanisms to perceive salient and camouflaged objects, existing models struggle to disentangle these tasks. Specifically, salient object detection (SOD) models frequently misclassify camouflaged objects as salient, while camouflaged object detection (COD) models conversely misinterpret salient objects as camouflaged. We hypothesize that this can be attributed to two factors: (i) the specific annotation paradigm of current SOD and COD datasets, and (ii) the lack of explicit attribute relationship modeling in current models. Prevalent SOD/COD datasets enforce a mutual exclusivity constraint, assuming scenes contain either salient or camouflaged objects, which poorly aligns with the real world. Furthermore, current SOD/COD methods are primarily designed for these highly constrained datasets and lack explicit modeling of the relationship between salient and camouflaged objects. In this paper, to promote the development of unconstrained salient and camouflaged object detection, we construct a large-scale dataset, USC12K, which features comprehensive labels and four different scenes that cover all possible logical existence scenarios of both salient and camouflaged objects. To explicitly model the relationship between salient and camouflaged objects, we propose a model called **USCNet**, which introduces two distinct prompt query mechanisms for modeling inter-sample and intrasample attribute relationships. Additionally, to assess the model's ability to distinguish between salient and camouflaged objects, we design an evaluation metric called CSCS. The proposed method achieves state-of-the-art performance across all scenes in various metrics. The code and dataset will be available at https://github.com/ssecv/ USCNet.

1. Introduction

The attention mechanism is one of the key cognitive functions of humans [52]. In real-world scenarios, people are of-

Table 1. Misinterpretation is prevalent when SOD/COD models applied across tasks. **Left:** Inference results of SOD models on COD datasets. VSCode uses the SOD prompt. **Right:** Inference results of COD models on SOD datasets. VSCode uses the COD prompt. The metric is F_{β}^{ω} . EV refers to the Expected Value.

SOD Models	COD Da	tasets	EV	COD Models	SOD 1	EV	
	COD10K	NC4K			DUTS	HKU-IS	
ICON [89]	0.6384	0.7522	0	SINet-V2 [12]	0.7412	0.7691	0
F3Net [68]	0.4327	0.6229	0	PFNet [45]	0.7361	0.7657	0
VSCode [41]	0.7145	0.8054	0	VSCode [41]	0.8614	0.8733	0

ten drawn to salient objects while overlooking camouflaged ones. From the perspective of the human visual recognition system, salient and camouflaged objects represent opposing concepts. The goal of Salient Object Detection (SOD) is to detect objects in an image that the human visual system considers most salient or attention-grabbing, while Camouflaged Object Detection (COD) aims to detect objects that are difficult to perceive or blend seamlessly with their surroundings [25]. In computer vision, these two tasks typically represent the model outputs using binary masks. Both of them exhibit significant potential across various fields, such as anomaly detection in medical image analysis [60], obstacle recognition in autonomous driving, camouflage detection in military reconnaissance [30], and wildlife tracking in environmental monitoring [57].

Existing SOD and COD methods have achieved remarkable progress in detecting salient and camouflaged objects. Some unified methods [25, 37, 41, 87] have improved the model's generalization ability in both SOD and COD tasks by jointly training SOD and COD datasets. However, we observe a counterintuitive phenomenon: although salient and camouflaged objects are conceptually opposing, SOD models frequently misclassify camouflaged objects as salient, while COD models conversely misinterpret salient objects as camouflaged. Such misdetections are undesirable and contradict the intended objectives of these two tasks.

To further validate this phenomenon, we select five models that used their original pre-trained weights to perform inference on four datasets. As shown in Table 1, the

SOD model, such as ICON [89], achieves an unexpectedly high F^{ω}_{β} of 0.6384 when inferring on the COD dataset COD10K [11], while the COD model, such as SINet-V2 [12], reaches 0.7412 on the SOD dataset DUTS [62]. The unified model VSCode [41], using the COD prompt, achieves 0.8733 on the SOD dataset HKU-IS. The false positive scores of these methods remain significantly higher than the expected value of 0.

We assume the first reason lies in the specific annotation paradigm of existing SOD and COD datasets.

While existing SOD and COD datasets have significantly advanced their respective fields through specialized design, they impose strict constraints, assuming that scenes contain either salient or camouflaged objects and providing only a single type of attribute label. For instance, in COD datasets, certain scenarios include salient objects, yet these objects are categorized as background simply because they are non-camouflaged. As a result, COD models become insensitive to salient objects, failing to accurately delineate the boundaries of the saliency feature space. A similar issue arises in SOD models. This specialized annotation paradigm presents even greater challenges for unified models that aim to address both tasks, as objects with identical visual characteristics may receive conflicting labels across different dataset types. Specifically, salient objects are labeled as background in COD datasets while remaining labeled as salient in SOD datasets, and the same inconsistency applies to camouflaged objects. Such labeling discrepancies may theoretically lead to information loss during the multi-task learning process, impairing the model's ability to generalize effectively.

In this paper, our goal is to advance the development of unconstrained salient and camouflaged object detection, enabling the model to detect objects in all possible logical scenarios of both salient and camouflaged objects. To achieve this, we construct a new dataset named USC12K. The dataset consists of 12,000 images with complete annotations, covering four scenes that encompass all logically possible cases of the existence of salient and camouflaged objects. In addition to the correction and optimization of existing datasets, we also collect and manually annotate 2,617 images containing both salient and camouflaged objects, and 1,436 images containing neither, from the internet, to ensure a balanced distribution across the four scenes. We evaluate 21 methods relevant to SOD and COD tasks on USC12K to establish a comprehensive benchmark for unconstrained salient and camouflaged object detection, aiming to drive further research in SOD and COD.

We assume the second reason lies in the absence of adaptive mechanisms for attribute relationship modeling under unconstrained conditions. The existing SOD and COD models have achieved significant success in single-task performance. However, they are primarily de-

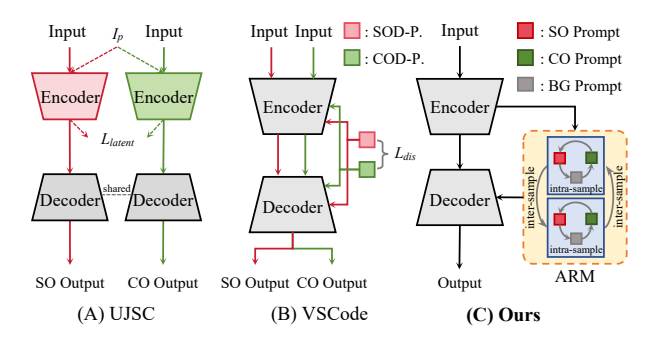


Figure 1. Architecture comparisons of unified models. SOD-P and COD-P represent prompts for the SOD and COD tasks. SO prompt, CO prompt, and BG prompt represent prompts for the salient, camouflaged, and background attributes.

signed for restricted, single-scene datasets, and the detection strategy focused on a single attribute of objects is not conducive to adapting to the detection of objects exhibiting two opposite visual modes. Although unified models achieve the detection of both object attributes by sharing network components, their process remains suboptimal for unconstrained salient and camouflaged object detection. Specifically, they typically employ a separate approach to learn the detection of salient and camouflaged objects, which is designed for previously constrained datasets. Although some models attempt to establish connections between the two attributes through techniques such as contrastive learning, as shown in Figure 1, UJSC [25] minimizes the Latent Space Loss L_{latent} to increase the distance between the distributions of the salient encoder and camouflaged encoder feature spaces on an additional dataset I_n . Similarly, VSCode [41] minimizes the Discrimination Loss L_{dis} to reduce the similarity between the salient and camouflaged prompts. However, they still lack explicit modeling of the relationship between salient and camouflaged objects within the network, and their loss functions are designed to model inter-sample relationships between saliency and camouflage outside the network, without capturing attribute relationships within individual samples. As a result, these models are unable to effectively learn their deep commonalities and differences in unconstrained scenarios.

To explicitly model the relationship between salient and camouflaged objects in unconstrained scenarios, we propose a network with a unified optimization pipeline, named Unconstrained Salient and Camouflaged Net (USCNet), which has the following two advantages: 1) USCNet employs an attribute prompt framework based on SAM, incorporating a SAM encoder with an adapter to leverage SAM's scene generalization capabilities and enhance adaptability in complex scenarios. 2) An Attribute Relation Modeling (ARM) module is introduced to model the relationship of saliency and camouflage combined with two complementary prompt queries: Inter-SPQ learns general features and captures global information by modeling attribute relation-

ships between samples, while Intra-SPQ models attribute relationships within a sample by focusing on its contextual information to learn the specific relationship between salient and camouflaged objects within the same sample. Inter-SPQ learns general features and captures global information by modeling attribute relationships between samples, while Intra-SPQ models attribute relationships within a sample by focusing on its contextual information to learn the specific relationship between salient and camouflaged objects within the same sample.

Moreover, existing metrics fail to quantify the model's confusion between salient and camouflaged objects, as they mainly evaluate the degree of foreground-background separation, such as weighted F-measure [44]. To fill this gap, we design a metric called Camouflage-Saliency Confusion Score (CSCS) to evaluate the model's ability to distinguish salient from camouflaged objects.

In summary, our contributions are listed as follows:

- We construct a large-scale unconstrained salient and camouflaged object detection dataset, USC12K, with comprehensive annotations. To our knowledge, this is the first dataset that is unconstrained regarding the existence of salient and camouflaged objects.
- We propose a SAM-based model, USCNet, with an ARM module to learn attribute relationships and two query types for modeling inter- and intra-sample relationships.
- A new metric, CSCS, is introduced to assess the model's confusion between salient and camouflaged objects.
- We evaluated 21 related methods on the USC12K, establishing a comprehensive benchmark. Our model achieved SOTAs performance across all metrics in all scenarios.

2. Related Work

2.1. Salient and Camouflaged Object Detection

Classic SOD and COD. In recent years, salient object detection models have focused on better detecting salient objects in images using various approaches. The main approaches can be divided into attention-based methods [34, 51, 85], multi-level feature-based methods [13, 19, 47, 65, 86], and recurrent-based methods [7, 33, 63]. Saliency detection [35, 83, 86, 89] primarily focuses on achieving saliency predictions while preserving the structure. Compared to SOD methods, current COD methods [12, 16, 22, 45, 48] focus primarily on edge-aware perception and texture perception. They are mainly divided into the following two types: multi-level feature-based methods [55, 77, 81, 84] and edge joint learning [16, 59, 80]. Both the SOD and COD models are designed for two tasks independently and lack modeling of the relationship between the two.

Unified. Recently, some works [25, 37, 41, 87] have already begun to unify the two tasks and attempt to establish connections between the two tasks. VSCode [41] learns

discriminative salient prompts and camouflage prompts by minimizing the cosine similarity between SOD and COD task prompts. UJSC [25] introduces the additional PAS-CAL VOC 2007 dataset to enhance the separation between the salient feature extractor and the camouflage feature extractor. Spider [87] distinguishes different attributes of the target by mining foreground/background-related semantic cues in the global context. EVP [37] learns task-specific visual prompts to distinguish salient and camouflaged objects. While existing unified models still struggle to distinguish between salient and camouflaged objects due to the lack of directly modeling the relationship between saliency and camouflage, we address this limitation by introducing an ARM module to explicitly model their relationship via inter-sample and intra-sample interactions.

2.2. Applications of SAM

The Segment Anything Model (SAM) [23] represents a significant advancement in scene segmentation using large vision models. Current works leveraging SAM [2, 43, 73, 82] showcase its adaptability to downstream tasks, notably in areas where traditional segmentation models struggle, such as EfficientSAM [73] and MedSAM [43]. More recently, the release of SAM2 [54] enhances the original SAM's ability to handle video content while demonstrating improved segmentation accuracy and inference efficiency in image segmentation across various downstream applications [29, 40, 75, 88]. Some works that use SAM for SOD and COD are closely related to our research. MDSAM [14] is a multi-scale and detail-enhanced SOD model based on SAM, aimed at improving the performance and generalization capability of the SOD task. SAM-Adapter [2] and SAM2-Adapter [3] offer a parameter-efficient finetuning way to enhance the performance of SAM and SAM2 in downstream tasks by adding task-specific knowledge. Building on the strong generalization capabilities of SAM, we strive to explore its capacity for detecting salient and camouflaged objects in unconstrained scenarios.

3. The Proposed USC12K Dataset

The current datasets for camouflaged object detection, such as COD10K [11], CAMO [24], NC4K [42], primarily feature scenes with exclusively camouflaged objects. Similarly, datasets for salient object detection, such as DUTS [62] and HKU-IS [27], predominantly focus on scenes with solely salient objects. Samples containing both salient and camouflaged objects are extremely scarce. Moreover, even when a small number of samples with both salient and camouflaged objects are available, only one attribute of the objects is annotated, which hinders the realization of unconstrained salient and camouflaged object detection. Therefore, we introduce the USC12K, a dataset that includes more comprehensive and complex scenarios

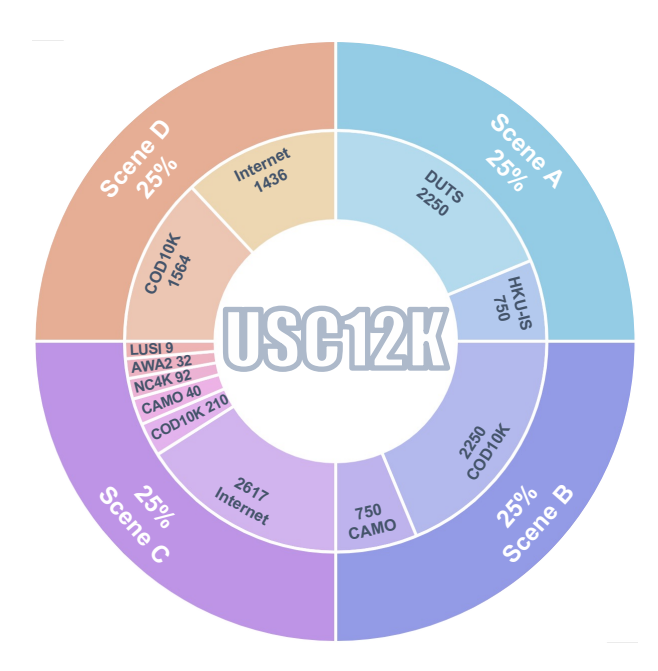


Figure 2. The data sources and distribution of the four scenes.

for unconstrained salient and camouflaged object detection. It includes scenes with both salient and camouflaged objects, scenes with only one type, and scenes without either. We will describe the details of USC12K in terms of three key aspects, as follows.

3.1. Data Collection

Under the premise of ensuring sample balance, we collect 12,000 images from 8 different sources and divide them into four scenes after manual filtering: (A) Scenes with only salient objects: 3,000 images containing only salient objects selected from SOD datasets DUTS and HKU-IS; (B) Scenes with only camouflaged objects: 3,000 images containing only camouflaged objects selected from COD datasets COD10K and CAMO; (C) Scenes with both salient and camouflaged objects: 342 images from the COD datasets COD10K, CAMO, and NC4K, along with 41 images from the datasets LSUI [49] and AWA2 [70], and an additional 2,617 images collected from the internet, making a total of 3,000 images; (D) Scenes without salient and camouflaged objects, considered as background: 1,564 images from COD10K, and 1,436 images from the internet, making a total of 3,000 images. Each scene has been meticulously reviewed by human annotators to ensure correct scene classification. Finally, we get 12,000 images, with the training set containing 8,400 images and the test set containing 3,600 images. The data source is shown in Figure 2.

3.2. Data Annotation

For the data with finalized scene classification, we retain the original labels for Scene A and B. For Scene C, we utilize SAM [23] to supplement masks for data with single-

Table 2. Data analysis of existing datasets.

Dataset	#Ann. IMG	Class	Scene A	Scene B	Scene C	Scene D
SOD [46]	300	-	300	X	X	X
PASCAL-S [28]	850	-	850	X	X	X
ECSSD [74]	1000	-	1000	X	X	X
HKU-IS [27]	4447	-	4447	X	X	X
MSRA-B [36]	5000	-	5000	X	X	X
DUT-OMRON [76]	5168	-	5168	X	X	X
MSRA10K [5]	10000	-	10000	X	X	X
DUTS [62]	15572	-	15572	X	X	X
SOC [9]	3000	80	3000	X	X	X
CAMO [24]	1250	8	X	1250	X	X
CHAMELEON [56]	76	-	X	76	X	X
NC4K [42]	4121	-	X	4121	X	X
COD10K [11]	7000	78	X	5066	X	1934
USC12K(Ours)	12000	179	3000	3000	3000	3000

attribute masks, while manually annotating masks for images collected from the internet. During category annotation, we set all pixels outside the mask of the entire dataset to 0. We obtain an initial coarse classification using CLIP [53], followed by manual verification and refinement. Except for images collected from COD10K [11], which already include camouflage object category labels, all other objects require classification. Some examples of different scenes from our USC12K dataset are shown in Figure 3. Then we assign category labels to each image, covering 9 super-classes and 179 sub-classes. Figure 3 in Appendix. §5 illustrates the class breakdown of our USC12K dataset.

3.3. Data Analysis

For deeper insights into SOD and COD datasets, we compare our USC12K against 13 other related datasets including: (1) nine SOD datasets: SOD [46], PASCAL-S [28], ECSSD [74], HKU-IS [27], MSRA-B [36], DUT-OMRON [76], MSRA10K [5], DUTS [62], and SOC [9]; (2) four COD datasets: CAMO [24], CHAMELEON [56], COD10K [11], and NC4K [42]; Table 2 shows the detailed information of these datasets. It can be seen that except for COD10K, all SOD datasets only contain salient objects, and nearly all COD datasets only contain camouflaged objects. The scenarios covered by these datasets are relatively limited. Notably, although the COD dataset COD10K contains some images with salient objects and images without any objects, these images lack labels and are not included in the training process. In contrast, the USC12K dataset we propose imposes no restrictions on scenes and includes labels for three attributes: saliency, camouflage, and background, with a well-balanced distribution.

4. The Proposed USCNet Baseline

Overview. As illustrated in Figure 4, the main components of the proposed USCNet include: (1) A SAM image encoder to extract object feature representation with adapter layers. (2) An Attribute Relation Modeling (ARM) module that generates three attribute prompts (saliency, camou-

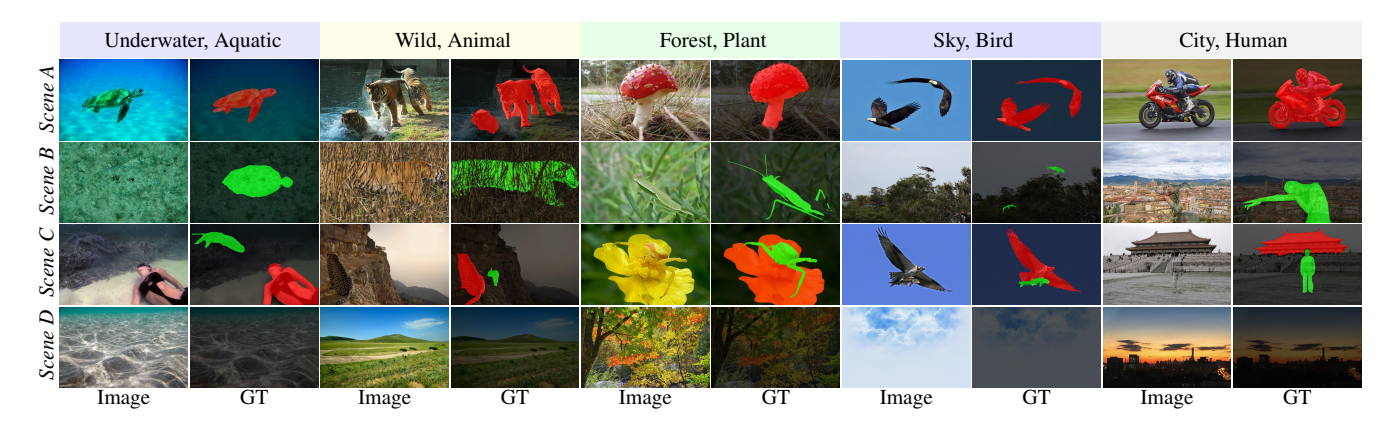


Figure 3. Example images from the USC12K dataset: Scene A: Only camouflaged object. Scene B: Only salient object. Scene C: Both salient and camouflaged objects simultaneously. Scene D: Background, none of them. More examples can be found in Appendix.§5

flaged, background), enables interactions within the module, and introduces two distinct prompt query mechanisms to model attribute relationships at both inter-sample and intra-sample levels. (3) A frozen mask decoder of SAM that is applied to predict the final saliency, camouflage, and background masks based on different attribute prompts.

4.1. SAM Encoder with Adapter

SAM [23] consists of an image encoder, a prompt encoder, and a mask decoder. In USCNet, we utilize the prompt architecture of SAM for identifying three attributes: saliency, camouflage, and background. The attribute prompts are generated by a designed ARM module, eliminating the need for the manual prompt. Each attribute prompt is mapped to a distinct binary mask. Following SAM-Adapter [2], USCNet integrates adapters into each layer of the SAM encoder with a parameter-efficient fine-tuning approach, as depicted in Figure 4. Through this approach, USC-Net blending SOD- and COD-specific knowledge with the general knowledge acquired by the larger model, better adapts to unconstrained scenes.

4.2. Attribute Relation Modeling

To elucidate the intricate relationship between saliency and camouflage in unconstrained scenarios, we introduce the Attribute Relation Modeling (ARM) module.

Our insight is that modeling the relationship of salient and camouflaged objects in unconstrained scenes necessitates the consideration of interactions across two dimensions: (i) Inter-sample relationship modeling: Salient and camouflaged objects often exhibit distinct features across samples. Modeling their inter-sample relationships helps identify universal discriminative features, such as size, location, color, and texture, crucial for distinguishing between them. (ii) Intra-sample relationship modeling: In complex scenarios where salient and camouflaged objects coexist, inter-sample modeling alone may be inadequate. For ex-

ample, when salient and camouflaged objects share similar colors or categories, intra-sample contextual information becomes essential for accurate differentiation. Building upon this foundation, we introduce ARM, a module that synergistically integrates both Inter-Sample Prompt Query (Inter-SPQ) and Intra-Sample Prompt Query (Intra-SPQ) to discriminatively query attribute-specific prompts across different samples and within individual samples, respectively. The Inter-SPQ is designed to extract generic features between samples, capturing attributes that are universally common across all samples, while the Intra-SPQ concentrates on extracting features within individual samples, emphasizing the distinctive contextual information inherent to each specific sample.

The Inter-SPQ consists of a set of learnable query embeddings $Q_{S_r} \in \mathbb{R}^{N \times C}, \ Q_{C_r} \in \mathbb{R}^{N \times C}$, and $Q_{B_r} \in \mathbb{R}^{N \times C}$, where N represents the number of queries, and Crepresents the dimensionality of the queries. The Inter-SPQ remains unchanged during inference, regardless of the specific sample. The generation of Intra-SPQ proceeds as follows: Initially, the feature F is extracted from the encoder and passed through an attention head composed of two 3 \times 3 convolutional layers to generate an attention map. The attention map is supervised by the ground truth to encourage it to focus on the salient and camouflaged regions within the image. Subsequently, the sigmoid function is applied to each channel of the attention map. This processed attention map is element-wise multiplied with the original feature F to isolate attribute-specific features. These features are subsequently passed through a linear layer to perform downsampling, generating the Intra-SPQ, which ensures dimensionality consistency with the Inter-SPQ. The Intra-SPQ changes during inference based on variations in the sample. The Intra-SPO generation process can be described by the following formula:

$$[Q_{S_a},Q_{C_a},Q_{B_a}]=Linear(\sigma(\Phi_{AH}(F))\otimes F), \qquad (1)$$
 where $Q_{S_a},~Q_{C_a},~{\rm and}~Q_{B_a}$ represent the Intra-SPQ for

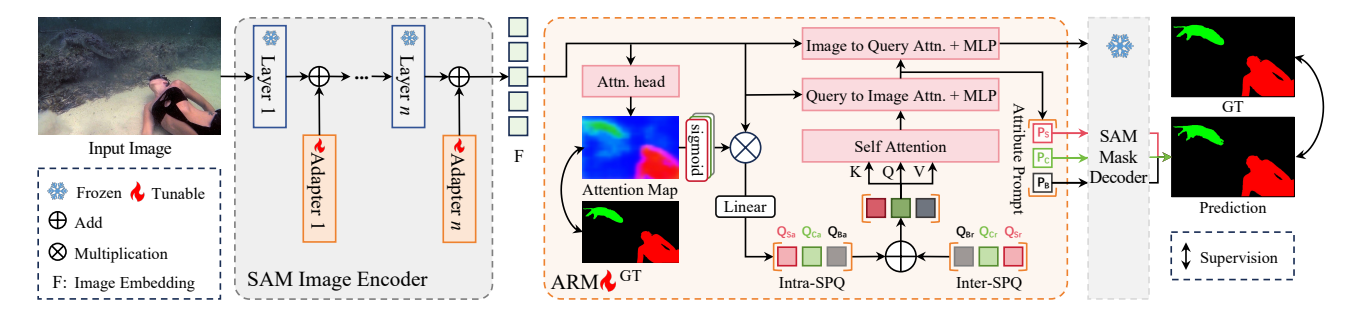


Figure 4. Architecture of our USCNet. USCNet includes: SAM image encoder with adapter, ARM module, and frozen SAM mask decoder.

saliency, camouflage, and background, respectively. σ denotes the sigmoid function, and Φ_{AH} represents the attention head. The \otimes denotes element-wise multiplication.

The Intra-SPQ captures feature information from specific images, whereas the Inter-SPQ discerns the fundamental differences among attributes. By integrating these two components through summation, our ARM is endowed with the capability to handle unconstrained scenarios, regardless of the presence of salient or camouflaged objects. Subsequently, we employ self-attention (SA) to establish relationships between queries and query-to-image (Q2I) attention to interact with the image embedding F, ultimately generating attribute prompts: $P = \{P_S \in \mathbb{R}^{N \times C}, \ P_C \in \mathbb{R}^{N \times C}, \ P_B \in \mathbb{R}^{N \times C}\}$. The process can be formulated as follows:

$$P = MLP(Q2I(SA(Intra-SPQ + Inter-SPQ), F)),$$
 (2)

where Q2I denotes the cross-attention from queries to the image embedding F, enabling the model to focus on relevant parts of the input based on the queries. Furthermore, we use image-to-query (I2Q) attention to focus on features related to attributes. Based on the three attribute-specific prompts fed into the pre-trained mask decoder in SAM, three masks— M_S , M_C , and M_B —are obtained, representing the predicted saliency, camouflage, and background, respectively. The process can be described as:

$$[M_S, M_C, M_B] = MaskDe([P_S, P_C, P_B], F), \qquad (3)$$

where MaskDe denotes the frozen SAM mask decoder. Finally, a softmax function is applied to the three masks to generate the final prediction.

4.3. Loss Function

We use the ground truth to supervise the final prediction and attention map. The total loss function of USCNet can be defined as:

$$\mathcal{L}_{Total} = \lambda_p \mathcal{L}_{pred.} + \lambda_a \mathcal{L}_{att.}, \tag{4}$$

where $\mathcal{L}_{pred.}$ represents the loss of the prediction map and $\mathcal{L}_{att.}$ indicates the loss of the attention map in the ARM.

Both of them are calculated using the Focal loss [31]:

$$\mathcal{L}_{focal} = -\frac{1}{N} \sum_{i=1}^{N} \alpha_{t_i} (1 - p_{t_i})^{\gamma} \log(p_{t_i}), \tag{5}$$

where p_{t_i} is the predicted probability for the target class t_i , α_{t_i} is the weighting factor for class t_i (empirically set to 1:4:6 for background, salient, and camouflaged pixels based on their pixel count ratio), γ is the default value of 2 to account for the varying difficulty of different objects, and N is the number of samples. Besides, λ_p , and λ_a are empirically set to 1 and 0.5 respectively to balance the total loss.

5. USC12K Benchmark

We evaluate 21 relevant methods on USC12K to establish a comprehensive benchmark. All models are trained and tested on the training set of USC12K (8,400 images) and the test set of USC12K (3,600 images).

Metrics. USC12K benchmark involves three distinct attributes: saliency, camouflage, and background. We employ three established metrics for semantic segmentation: $\text{mAcc}\uparrow$, $\text{IoU}\uparrow$, and $\text{mIoU}\uparrow$ [39, 72]. Inspired by [26], we also employ AUC \uparrow , SI-AUC \uparrow , $F_m^{\beta}\uparrow$, SI- $F_m^{\beta}\uparrow$, $F_{\text{max}}^{\beta}\uparrow$, SI- $F_{\text{max}}^{\beta}\uparrow$, $E_m\uparrow$ to evaluate the model's capability in detecting objects of varying sizes. Additionally, to evaluate the model's ability to distinguish salient from camouflaged objects, we propose a novel metric, the Camouflage-Saliency Confusion Score (CSCS \downarrow), which is formulated as follows:

$$CSCS = \frac{1}{2} \left(\frac{\mathcal{P}_{CS}}{\mathcal{P}_{BS} + \mathcal{P}_{SS} + \mathcal{P}_{CS}} + \frac{\mathcal{P}_{SC}}{\mathcal{P}_{BC} + \mathcal{P}_{SC} + \mathcal{P}_{CC}} \right), (6)$$

where $\mathbb{P}=\{\mathcal{P}_{\lambda\theta}\,|\,\lambda\in\Theta,\theta\in\Theta\}$, $\Theta=\{B,C,S\}$, the B, C and S denote background, camouflage, and saliency, \mathcal{P}_{CS} represents regions where camouflage is predicted as salient, while \mathcal{P}_{SC} represents regions where saliency is predicted as camouflage; both are regions of confusion. A lower CSCS indicates a stronger robustness to distinguish between salient and camouflaged objects. More details of CSCS can be seen in Appendix. §1.

Competitors. We compare with 21 related models, including (I) SOD models: GateNet [86], F3Net [68], MSFNet [83], VST [35], EDN [69], ICON [89], MD-SAM [14]; (II) COD models: SINet-V2 [12], PFNet [45],

Table 3. Quantitative comparisons with 21 related methods for SOD and COD. $IoU_S\uparrow$: IoU score for salient objects. $IoU_C\uparrow$: IoU score for camouflaged objects. The best two scores are highlighted in **red** and **green**, respectively. All metrics presented in the table are expressed as percentages (%). We use $mIoU\uparrow$, $mAcc\uparrow$, and $CSCS\downarrow$ to evaluate the models in overall scenes.

Task	Model	Venue	Update	Scene A	Scene B	Sce	ne C		o	verall Scer	ies	
Task	Model	venue	Para.(M)	IoU_S	IoU_C	IoU_S	IoU_C	IoU_S	IoU_C	mIoU	mAcc	CSCS
	GateNet [86]	ECCV'20	128	68.32	54.26	66.85	35.03	65.08	44.17	68.27	78.07	11.30
	F3Net [68]	AAAI'20	26	70.05	52.62	67.20	36.38	66.12	44.81	68.80	77.86	9.36
	MSFNet [83]	MM'21	28	70.14	54.78	69.92	36.64	66.69	45.89	69.40	79.77	9.90
SOD	VST [35]	ICCV'21	43	68.14	49.82	61.61	22.56	63.18	38.45	65.55	74.77	11.30
300	EDN [69]	TIP'22	43	71.59	57.94	69.37	37.70	68.00	48.27	70.70	80.60	9.23
	PGNet [71]	CVPR'22	73	74.69	57.31	71.94	37.21	70.72	48.78	71.82	80.76	7.71
	ICON [89]	TPAMI'22	32	68.09	50.57	67.48	30.65	65.86	45.53	68.99	79.53	10.24
	MDSAM [14]	MM'24	14	72.96	56.16	67.21	36.06	69.67	49.05	71.67	82.92	10.21
	SINet-V2 [12]	TPAMI'21	27	72.96	56.16	67.21	36.06	69.50	47.47	70.20	79.58	8.83
	PFNet [45]	CVPR'21	47	69.07	52.83	67.20	32.81	65.73	43.76	68.30	78.00	10.04
	ZoomNet [48]	CVPR'22	33	74.11	51.12	66.79	29.69	66.43	43.28	68.35	77.72	8.88
	FEDER [16]	CVPR'23	44	74.35	58.04	67.66	32.26	68.65	46.46	70.32	81.27	10.01
	PRNet [20]	TCSVT'24	13	76.10	61.54	60.10	32.16	68.68	50.88	71.87	82.89	8.40
COD	ICEG [17]	ICLR'24	100	73.67	68.38	68.43	44.33	69.22	58.71	74.68	83.53	8.16
	CamoDiffusion [4]	AAAI'24	72	75.01	59.39	53.49	45.03	63.49	52.80	70.70	77.73	7.73
	CamoFormer [78]	TPAMI'24	71	75.88	66.19	73.33	44.14	71.86	56.09	74.81	84.17	7.57
	PGT [64]	CVIU'24	68	72.75	61.51	70.01	41.21	71.46	56.83	75.03	83.35	9.09
	SAM-Adapter [2]	ICCVW'23	4.11	78.90	67.69	68.19	27.73	70.66	52.69	73.38	83.35	10.28
	SAM2-Adapter [3]	arXiv'24	4.36	78.75	70.28	69.01	38.20	71.42	56.71	74.98	84.74	9.12
	EVP [37]	CVPR'23	4.95	75.85	59.81	71.41	37.64	70.30	50.36	72.16	79.96	8.67
Unified	VSCode [41]	CVPR'24	60	76.04	60.31	72.58	39.46	71.08	55.14	74.17	84.01	8.17
	USCNet (Ours)	-	4.04	79.70	74.99	74.80	45.73	75.57	61.34	78.03	87.92	7.49

Table 4. After training with USC12K, misinterpretation is largely eliminated. **Left:** Inference results of SOD models on COD datasets. VSCode uses the SOD prompt. **Right:** Inference results of COD models on SOD datasets. VSCode uses the COD prompt. The metric is F_{β}^{ω} . EV refers to the Expected Value.

SOD Models	COD Da		EV	COD Models	SOD 1	EV	
	COD10K	NC4K			DUTS	HKU-IS	
ICON [89]	0.0146	0.0834	0	SINet-V2 [12]	0.0708	0.0443	0
F3Net [68]	0.0129	0.0787	0	PFNet [45]	0.1152	0.0874	0
VSCode [41]	0.0097	0.0626	0	VSCode [41]	0.0537	0.0391	0

Table 5. Generalization performance of six methods on SOD dataset: DUTS, HKU-IS and COD dataset: NC4K and COD10K. More comparisons can be found in Appendix. §3.

Model	DU	TS	нк	U-IS	NC4	4K	COD10K		
Model	$F_{\beta}^{\max} \uparrow$	$E_{\phi}^{\mathrm{m}}\uparrow$							
ICON [89]	.679	.785	.814	.874	.540	.715	.631	.752	
F3Net [68]	.703	.794	.832	.881	.576	.744	.661	.773	
SINet-V2 [12]	.732	.821	.838	.884	.609	.763	.662	.769	
PFNet [45]	.691	.790	.818	.876	.556	.730	.660	.769	
VSCode [41]	.724	.812	.834	.885	.626	.787	.684	.783	
USCNet	.784	.852	.844	.886	.794	.877	.743	.869	

ZoomNet [48], FEDER [16], ICEG [17], PRNet [20], CamoDiffusion [4], CamoFormer [78], PGT [64], SAM-Adapter [2] and SAM2-Adapter [3]; (III) Unified methods: VSCode [41] and EVP [37].

Technical Details. All models are retrained on the USC12K training set at a resolution of 352×352 . Horizontal flipping and random cropping are applied for data augmentation. Experiments are conducted on one NVIDIA

L40 GPU. The number of trained parameters for all models is detailed in Table 3. We use the hiera-large version of SAM2 following the SAM2-Adapter [3]. AdamW optimizer with warm-up and linear decay is used. The initial learning rate is set to 0.0001. The batch size is set to 24, and the maximum number of epochs is set to 90. More technical details of all methods can be found in Appendix. §4.

5.1. Quantitative Evaluation

Performance on USC12K. We present in Table 3 the performance of compared models on the USC12K benchmark. Comparing the results of the models in single-attribute scenes (refer to Scene A and Scene B) with those in multiattribute scenes (refer to Scene C) reveals that all models achieve lower scores in Scene C than in Scene A and Scene B. This indicates that the simultaneous presence of both salient objects and camouflaged objects increases the difficulty for the models to recognize both. Our method achieves a greater lead in overall scenes, demonstrating that our model is more adaptable when faced with more challenging scenarios. Furthermore, USCNet achieves the best performance in all scenarios compared to all other compared methods. Additionally, the evaluation results for other metrics, including AUC \uparrow , SI-AUC \uparrow , F_m^{β} \uparrow , SI- F_m^{β} \uparrow , F_{\max}^{β} \uparrow , SI- F_{\max}^{β} \uparrow , E_m \uparrow , can be found in Table 1 and Table 2 in Appendix. §2.

Misdetection performance. To explore the impact of training with the USC12K dataset on the model's false detection rate, we test the SOD and COD models on the COD and SOD datasets. The results in Table 4 show that training with

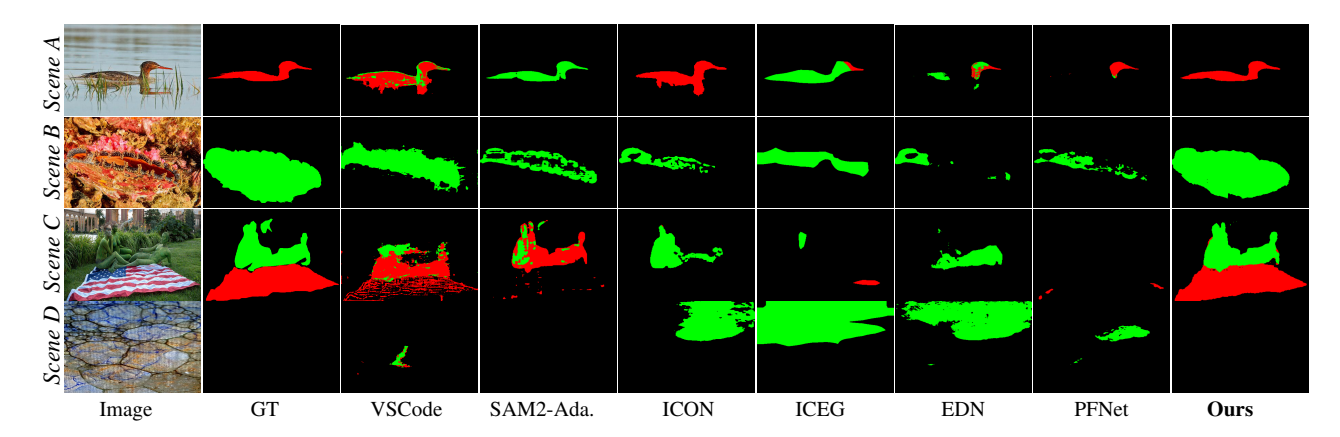


Figure 5. Qualitative comparisons of USCNet with five models across overall scenes. More visualization can be seen in Appendix. §6.

Table 6. Effectiveness of different components in ARM. Intra-S.: intra-sample prompt query. Inter-S.: inter-sample prompt query.

Encoder	Decoder	Intra-S.	Inter-S.	Q2I	I2Q	Para.	IoU_S	$ IoU_C$	mIoU	mAcc	CSCS
Frozen	Tuning	X	X	X	X	4.22	66.42	44.02	68.78	77.65	11.58
Tuning	Tuning	X	X	X	X	4.36	71.42	56.71	74.98	84.74	9.12
Tuning	Frozen	X	•	/	/	3.44	71.68	57.53	75.31	85.15	9.07
Tuning	Frozen	V	X	/	~	4.03	74.32	58.91	76.96	85.80	7.98
Tuning	Frozen	•	V	X	X	0.75	70.97	56.56	74.77	84.43	9.85
Tuning	Frozen	~	~	/	X	2.40	73.08	58.45	76.73	85.63	8.52
Tuning	Frozen	V	V	/	/	4.04	75.57	61.34	78.03	87.92	7.49

USC12K significantly reduced the model's false detection score compared to Table 1.

Generalization performance. We evaluate the model's performance across six widely used datasets. This includes COD datasets like COD10K, NC4K, and CAMO-TE, as well as SOD datasets like DUT-TE, HKU-IS, and DUT-OMRON. Our model demonstrates stronger generalization ability. The results are shown in Table 5 and Appendix. §3.

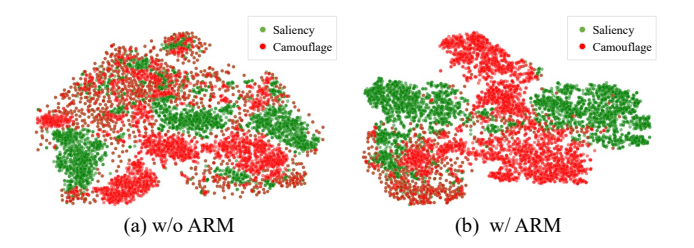


Figure 6. Embedding visualization of salient and camouflaged objects in USC12K test set images by our model w/o and w/ the ARM module. Dimensions reduced using t-SNE [61].

5.2. Qualitative Evaluation

In Figure 5, we compare our model's qualitative results with six models. Our method exhibited a better detection capability for salient and camouflaged objects in all scenes. Benefiting from the ARM module, our method better distinguished salient objects and camouflaged objects in the same image within Scene C of Figure 5. For Scene D, SOD and

COD methods become confused when encountering backgrounds, resulting in poor performance and unstable robustness, whereas our model demonstrates better performance.

5.3. Ablation Study

Effectiveness of Different Components in ARM. As shown in Table 6, ablation studies on overall scene validate the effectiveness of the ARM module's components. From Line 3, 4, and 7, it is evident that both Intra-SPQ and Inter-SPQ improve the performance of the model, with Intra-SPQ providing a greater performance enhancement than Inter-SPQ when used together, achieving optimal results. Line 5, 6, and 7 demonstrate that Q2I and I2Q also facilitate the distinction of salient camouflaged objects, leading to reductions in CSCS of 2.36% and 1.08%, respectively. Additionally, compared to the original SAM2 (refer to Line 1) and SAM2-Adapter (refer to Line 2), the proposed USCNet enhances performance on the USC12K task across all metrics through a more efficient fine-tuning approach by incorporating the ARM module and frozen mask decoder.

Impact of ARM on Embedding Separation. We further demonstrate the effectiveness of the ARM module by visualizing embeddings of the salient and camouflaged objects. As shown in Figure 6, the plot without ARM module is homogeneous, mixing salient and camouflaged object embeddings. In contrast, our model with the ARM module produces a more distinct and well-clustered representation, better separating the embeddings of salient and camouflaged objects. More ablation can be seen in Appendix. §7.

6. Conclusion

We analyze the misdetection of salient and camouflaged objects in current SOD and COD methods, and pinpoint the constraints of existing datasets and the models. A large-scale dataset named USC12K to advance unconstrained salient and camouflaged object detection. Accordingly, we design a unified pipeline USCNet to explicitly models both inter-sample and intra-sample attribute relation-

ships. In addition, we propose a new evaluation metric, CSCS, to assess the model's confusion between camouflage and saliency. Extensive experiments demonstrate that the proposed dataset alleviates the models' misdetection issue, and our method outperforms existing related models on the USC12K benchmark, showing better generalization across six SOD and COD datasets. We believe that the USC12K benchmark will promote further research in SOD and COD, helping models better capture saliency and camouflage patterns that align with the human visual system.

Appendix

We summarize the supplementary material from the following aspects:

Table of contents:

- §7: CSCS Metric
- §8:Performance in Detecting Objects of Different Sizes
- §9: Results on Popular COD and SOD Datasets
- §10: More Technical Details
- §11: More USC12K Dataset Detail and Examples
- §12: Additional Qualitative Results
- §13: Additional Ablation Study

7. CSCS Metric

Contrary to the Intersection over Union (IoU) that measures accuracy for a single class, the Camouflage-Saliency Confusion Score (CSCS) assesses the misclassification between two distinct classes. The CSCS, designed to evaluate the confusion between camouflaged and salient objects, is calculated as follows:

$$CSCS = \frac{1}{2} \left(\frac{\mathcal{P}_{CS}}{\mathcal{P}_{BS} + \mathcal{P}_{SS} + \mathcal{P}_{CS}} + \frac{\mathcal{P}_{SC}}{\mathcal{P}_{BC} + \mathcal{P}_{SC} + \mathcal{P}_{CC}} \right), (7)$$

where $\mathbb{P}=\{\mathcal{P}_{\lambda\theta}\,|\,\lambda\in\Theta,\theta\in\Theta\}$, $\Theta=\{B,C,S\}$, the B, C and S denote background, camouflage and saliency. A lower CSCS value indicates a stronger ability of the network to discriminate between salient and camouflaged objects. \mathcal{P}_{CS} represents the label as camouflage but is predicted as saliency. We aim to minimize the misclassification of camouflaged pixels as salient, ensuring the network correctly distinguishes between camouflaged and salient objects. The same applies to \mathcal{P}_{SC} . As shown in Figure 8, we present the confusion matrix of the proposed USCNet on the USC12K test set. Our model balances improvements across all metrics, achieving a mIoU of 0.775 and a CSCS of 0.0749 (see Table 3 in the manuscript).

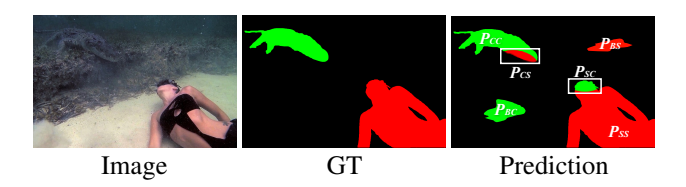


Figure 7. The illustration of \mathcal{P}_{BS} , \mathcal{P}_{SS} , \mathcal{P}_{CS} , \mathcal{P}_{BC} , \mathcal{P}_{SC} , and \mathcal{P}_{CC} in the CSCS metric. The **red** mask represents the salient regions, and the **green** mask denotes the camouflaged regions.

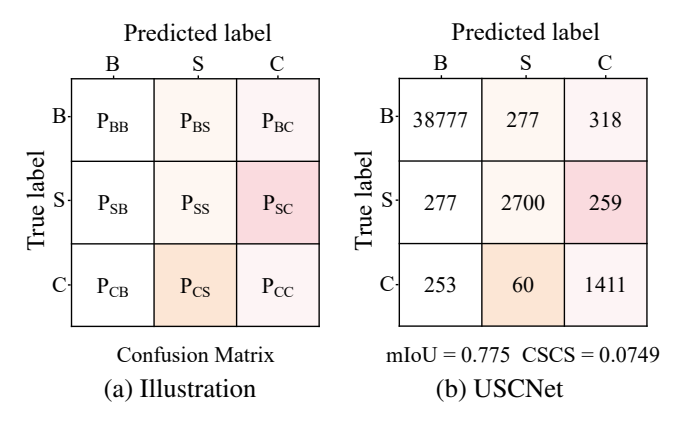


Figure 8. Confusion matrix of our USCNet on the USC12K test set. The units of the values in the confusion matrix are in tens of thousands (1E+04).

8. Performance in Detecting Objects of Different Sizes

To evaluate the model's ability to detect objects of varying sizes, we employ several metrics: AUC \uparrow , SI-AUC \uparrow , F_m^β \uparrow , SI- F_m^β \uparrow , Em \uparrow . From Table 7 and Table 8, it can be observed that, compared to the size-sensitive(e.g., AUC \uparrow and F_m^β \uparrow) and size-invariance metrics(e.g., SI-AUC \uparrow and SI- F_m^β \uparrow), our method exhibits smaller performance fluctuations, demonstrating its robustness to variations in object size and number in the scene.

9. Results on Popular COD and SOD Datasets

To further validate the effectiveness and robustness of our method regarding generalizability, we conduct tests on popular SOD datasets (DUTS [62], HKU-IS [27], and DUT-OMRON [76]) and COD datasets (CAMO [24], COD10K [11], and NC4K [42]), with all methods uniformly trained using our USC12K dataset. We adopt five metrics that are widely used in COD and SOD tasks [12, 66]. These metrics include maximal F-measure $(F_{\beta}^{\text{max}} \uparrow)$ [1], weighted F-measure $(F_{\beta}^{\omega} \uparrow)$ [44], Mean Absolute Error (MAE, $M \downarrow$) [50], Structural measure (S-measure, $S_{\alpha} \uparrow$) [8], and mean Enhanced alignment measure (E-measure, $E_{\phi}^{m} \uparrow$) [10]. As shown in Table 9 and Table 10, our USCNet achieves state-of-the-art performance on these datasets through parameter-efficient fine-tuning. This fur-

Table 7. Performance of different models detecting salient objects on USC12K testing set.

Task	Model	Update				USC12K-SOD			
Task	Model	Params(M)	AUC ↑	SI-AUC↑	$F_m^{\beta} \uparrow$	$SI-F_m^{\beta}\uparrow$	$F_{\mathrm{max}}^{eta}\uparrow$	$SI-F_{\max}^{\beta}\uparrow$	$E_m \uparrow$
	GateNet [86]	128	.810	.812	.696	.754	.706	.764	.775
	F3Net [68]	26	.828	.826	.722	.765	.734	.777	.803
SOD	MSFNet [83]	28	.832	.831	.726	.772	.735	.782	.805
SOD	VST [35]	43	.777	.777	.642	.732	.650	.741	.742
	EDN [69]	43	.831	.830	.726	.769	.736	.780	.804
	ICON [89]	32	.821	.832	.702	.764	.711	.774	.795
	SINetV2 [12]	27	.843	.842	.755	.783	.765	.793	.827
	PFNet [45]	47	.820	.822	.712	.756	.724	.767	.799
	ZoomNet [48]	33	.821	.823	.710	.765	.720	.774	.791
	FEDER [16]	44	.841	.842	.742	.784	.750	.796	.820
COD	ICEG [17]	100	.830	.825	734	.762	.743	.770	.831
	PRNet [20]	13	.851	.845	.742	.779	.750	.792	.832
	CamoFormer [78]	71	.844	.843	.750	.782	.758	.790	.821
	PGT [64]	68	.831	.828	.717	.773	.727	.784	.791
	SAM2-Adapter [3]	4.36	.847	.847	.741	.783	.751	.794	.816
	VSCode [41]	60	.843	.842	.749	.776	.768	.789	.822
Unified	EVP [37]	4.95	.850	.847	.751	.782	.771	.792	.830
	USCNet(Ours)	4.04	.853	.850	.761	.787	.772	.798	.833

Table 8. Performance of different models detecting camouflaged objects on USC12K testing set.

Task	Model	Update				USC12K-COD			
Task	Model	Params(M)	AUC↑	SI-AUC↑	$F_m^{\beta} \uparrow$	$SI-F_m^{\beta}\uparrow$	$F_{\max}^{\beta} \uparrow$	$SI-F_{\max}^{\beta}\uparrow$	$E_m \uparrow$
	GateNet [86]	128	.692	.687	.443	.558	.453	.569	.651
	F3Net [68]	26	.695	.687	.449	.564	.458	.574	.649
SOD	MSFNet [83]	28	.698	.691	.455	.565	.465	.576	.659
SOD	VST [35]	43	.626	.625	.303	.536	.312	.546	.524
	EDN [69]	43	.709	.703	.476	.575	.485	.585	.670
	ICON [89]	32	.663	.663	.384	.549	.394	.560	.587
	SINetV2 [12]	27	.715	.705	.505	.588	.514	.598	.690
	PFNet [45]	47	.678	.672	.429	.544	.440	.555	.630
	ZoomNet [48]	33	.657	.653	.394	.545	.405	.556	.588
	FEDER [16]	44	.710	.703	.486	.567	.497	.578	.689
COD	ICEG [17]	100	.730	.717	.525	.601	.532	.609	.719
	PRNet [20]	13	.705	.695	.454	.569	.464	.579	.652
	CamoFormer [78]	71	.756	.745	.565	.626	.575	.636	.743
	PGT [64]	68	.746	.734	.527	.596	.539	.607	.715
	SAM2-Adapter [3]	4.36	.770	.761	.575	.637	.585	.647	.746
-	VSCode [41]	60	.735	.727	.519	.601	.525	.597	.722
Unified	EVP [37]	4.95	.695	.684	.485	.577	.494	.587	.650
	USCNet(Ours)	4.04	.801	.794	.610	.658	.619	.667	.795

ther confirms the strong capability of our method to accurately identify both salient and camouflaged objects in unconstrained environments. This achievement is attributed to the exceptional versatility of SAM in class-agnostic segmentation tasks and the discriminative ability of our specially designed ARM for distinguishing between salient and camouflaged objects.

10. More Technical Details

All models are retrained using the training set of USC12K with an input image resolution of 352×352. Horizontal flipping and random cropping are applied for data aug-

mentation. The experiments are conducted in PyTorch on one NVIDIA L40 GPU. For our model, we use the hieralarge version of SAM2 following the SAM2-Adapter [3]. AdamW optimizer is used with a warm-up strategy and linear decay strategy. The initial learning rate is set to 0.0001. The batch size is set to 24, and the maximum number of epochs is set to 90.

Backbone of models. The models compared can be divided into two categories based on their papers: one is full-tuning models, and the other is parameter-efficient finetuning (PEFT) models. (i)Full Tuning models: Include all SOD and COD methods and VSCode in the Unified Method. For fairness, the models compared are all trained

Table 9. Generalization performance of related methods on the DUTS, HKU-IS, and DUT-OMRON test sets. \uparrow / \downarrow represents the higher/lower the score, the better.

Task	Model	Update]	DUTS				Н	IKU-IS				DUT	-OMRO	ON	
1dSK	Wiodei	Params(M)	$F_{\beta}^{\max} \uparrow$	$F^{\omega}_{\beta}\uparrow$	$M \downarrow$	$S_{\alpha} \uparrow$	$E_{\phi}^{\mathrm{m}}\uparrow$	$F_{\beta}^{\max} \uparrow$	$F^{\omega}_{\beta} \uparrow$	$M\downarrow$	$S_{\alpha} \uparrow$	$E_{\phi}^{\mathrm{m}}\uparrow$	$F_{\beta}^{\max} \uparrow$	$F^{\omega}_{\beta}\uparrow$	$M \downarrow$	$S_{\alpha} \uparrow$	$E_{\phi}^{\mathrm{m}}\uparrow$
	GateNet [86]	128	.666	.644	.062	.755	.765	.804	.785	.049	.841	.857	.634	.603	.079	.747	.751
	F3Net [68]	26	.703	.683	.055	.783	.794	.832	.816	.044	.853	.881	.638	.615	.073	.747	.758
SOD	MSFNet [83]	28	.651	.638	.063	.749	.758	.824	.806	.045	.853	.877	.641	.611	.076	.751	.764
SOD	VST [35]	43	.630	.610	.061	.744	.749	.777	.760	.052	.820	.851	.580	.560	.073	.720	.715
	EDN [69]	43	.692	.676	.053	.784	.785	.820	.806	.043	.852	.873	.616	.597	.071	.742	.735
	ICON [89]	32	.679	.647	.069	.769	.785	.814	.787	.051	.843	.874	.615	.576	.099	.728	.738
	SINetV2 [12]	27	.732	.710	.052	.801	.821	.838	.822	.046	.847	.884	.665	.642	.068	.763	.786
	PFNet [45]	47	.691	.668	.060	.775	.790	.818	.801	.048	.843	.876	.643	.614	.075	.747	.764
	ZoomNet [48]	33	.729	.709	.053	.801	.813	.785	.774	.051	.830	.842	.623	.601	.075	.742	.735
	FEDER [16]	44	.736	.714	.052	.808	.821	.839	.827	.045	.869	.881	.645	.615	.077	.755	.760
COD	PRNet [20]	13	.773	.756	.043	.830	.849	.840	.833	.044	.857	.880	.708	.685	.057	.796	.808
	ICEG [17]	100	.719	.700	.050	.789	.820	.832	.815	.045	.848	.896	.664	.645	.061	.762	.785
	CamoFormer [78]	71	.733	.715	.049	.813	.819	.838	.817	.046	.857	.884	.687	.661	.066	.783	.793
	PGT [64]	68	.686	.670	.053	.786	.779	.819	.802	.044	.855	.871	.642	.619	.068	.758	.754
	SAM-Adapter [2]	4.11	.761	.746	.048	.834	.796	.822	.806	.043	.836	.869	.708	.685	.059	.793	.802
	SAM2-Adapter [3]	4.36	.776	.762	.041	.831	.848	.831	.828	.042	.849	.881	.706	.692	.056	.790	.810
	VSCode [41]	60	.724	.706	.060	.795	.812	.834	.830	.043	.851	.885	.636	.608	.075	.748	.753
Unified	EVP [37]	4.95	.769	.750	.045	.833	.836	.835	.832	.043	.852	.878	.710	.692	.057	.794	.810
	USCNet(Ours)	4.04	.784	.780	.040	.835	.852	.844	.840	.042	.860	.886	.710	.697	.056	.796	.814

Table 10. Generalization performance of related methods on CAMO, COD10K, and NC4K test set. \uparrow / \downarrow represents the higher/lower the score, the better.

Task	Model	Update		(CAMO]	NC4K				C	OD10K		
1dSK	Wiodei	Params(M)	$F_{\beta}^{\max} \uparrow$	$F^{\omega}_{\beta} \uparrow$	$M\downarrow$	$S_{\alpha} \uparrow$	$E_{\phi}^{\mathrm{m}}\uparrow$	$F_{\beta}^{\max} \uparrow$	$F^{\omega}_{\beta} \uparrow$	$M\downarrow$	$S_{\alpha} \uparrow$	$E_{\phi}^{\mathrm{m}}\uparrow$	$F_{\beta}^{\max} \uparrow$	$F^{\omega}_{\beta} \uparrow$	$M\downarrow$	$S_{\alpha} \uparrow$	$E_{\phi}^{\mathrm{m}}\uparrow$
	GateNet [86]	128	.573	.542	.109	.666	.680	.562	.529	.047	.707	.724	.675	.645	.066	.752	.777
	F3Net [68]	26	.538	.506	.117	.643	.657	.576	.539	.047	.712	.744	.661	.633	.070	.738	.773
SOD	MSFNet [83]	28	.568	.535	.113	.661	.682	.543	.534	.052	.692	.719	.671	.645	.067	.747	.778
зов	VST [35]	43	.484	.455	.109	.636	.631	.468	.430	.055	.661	.670	.597	.567	.072	.710	.732
	EDN [69]	43	.573	.542	.109	.666	.680	.595	.562	.044	.727	.756	.688	.660	.063	.761	.795
	ICON [89]	32	.520	.481	.125	.641	.648	.540	.502	.053	.695	.715	.631	.596	.076	.724	.752
	SINetV2 [12]	27	.590	.562	.102	.681	.694	.609	.577	.043	.729	.763	.662	.639	.066	.740	.769
	PFNet [45]	47	.535	.505	.110	.652	.661	.556	.524	.049	.699	.730	.660	.633	.068	.737	.769
	ZoomNet [48]	33	.494	.472	.113	.635	.612	.520	.496	.048	.488	.671	.596	.576	.074	.708	.706
	FEDER [16]	44	.567	.538	.106	.669	.687	.636	.598	.042	.749	.793	.688	.664	.063	.758	.790
COD	PRNet [20]	13	.648	.607	.096	.716	.766	.709	.672	.059	.772	.820	.650	.603	.038	.756	.815
	ICEG [17]	100	.728	.697	.066	.769	.820	.735	.708	.051	.786	.840	.645	.610	.035	.753	.807
	CamoFormer [78]	71	.645	.618	.078	.732	.750	.729	.707	.054	.789	.822	.668	.639	.035	.770	.811
	PGT [64]	68	.635	.612	.089	.718	.730	.729	.706	.052	.791	.819	.642	.612	.036	.758	.786
	SAM-Adapter [2]	4.11	.661	.638	.080	.744	.753	.688	.667	.037	.788	.808	.727	.710	.051	.794	.809
	SAM2-Adapter [3]	4.36	.717	.692	.074	.779	.807	.724	.694	.044	.809	.847	.735	.694	.045	.819	.845
	VSCode [41]	60	.562	.532	.109	.658	.678	.626	.591	.043	.744	.787	.684	.662	.067	.753	.783
Unified	EVP [37]	4.95	.636	.637	.085	.701	.718	.693	.694	.040	.742	.775	.615	.614	.069	.724	.749
	USCNet(Ours)	4.04	.829	.790	.049	.845	.886	.794	.768	.039	.839	.877	.743	.700	.030	.821	.869

according to the configurations specified in their original papers. (ii)PEFT models: SAM-Adapter, SAM2-Adapter, EVP in the Unified Method and our model. The backbone architectures across various models consist of several types. For full tuning, VST employs a transformer encoder based on T2T-ViT [79], while SINet-V2 utilizes Res2Net-50 [15]. VSCode uses Swin-T [38], and ICEG adopts Swin-B [38]. PRNet is based on the SMT backbone [32], and both CamoDiffusion, CamoFormer, and PGT use PVTv2-

b4 [67]. Other models generally rely on ResNet-50 [18] with pre-trained weights from ImageNet [6]. In the case of PEFT models, EVP uses SegFormer-B4 [72] as its base, SAM-Adapter uses the default ViT-H version of SAM [23], and both SAM2-Adapter and our model employ the hieralarge version of SAM2 [54].

Training and Inference. For traditional SOD and COD models: USC12K is defined by three attributes: saliency, camouflage, and background. Conventional methods for

COD and SOD are crafted for dichotomous mapping tasks and don't seamlessly transition to the nuanced demands of the USC12K benchmark. Inspired by seminal works in semantic segmentations [39, 58], we retool the output layers of our models to yield a tripartite representation for saliency, camouflage, and background. This is achieved by harnessing a softmax layer to generate a predictive mapping. We employ a cross-entropy loss function to refine the model, which is congruent with our overarching methodological framework. For unified models: VSCode and EVP, which require task-specific prompts for each dataset, we create two copies of the USC12K training set. One copy is used for SOD, with the ground truth being the SOD-only mask, and is used to train the prompts corresponding to the SOD task. The other copy is used for COD, with the ground truth being the COD-only mask, and is used to train the prompts corresponding to the COD task. VSCode is trained once using all 16,800 images (two copies of 8,400 images), while EVP is trained twice on the two separate training sets (each containing 8,400 images) to obtain the two task-specific prompts. During inference, all unified models perform inference on the testing set of USC12K twice, with the corresponding prompt enabled for each task. The first inference run generates the SOD results, and the second inference run generates the COD results. The final prediction is obtained by merging the SOD and COD predictions. For overlapping pixels, the attribute with the higher prediction value between the two tasks is chosen as the final attribute for that pixel.

11. More USC12K Dataset Detail and Examples

Object category distribution. We obtain an initial coarse classification using CLIP [53], followed by manual verification and refinement. Except for images collected from COD10K [11], which already include camouflage object category labels, all other objects require classification. Then we assign category labels to each image, covering 9 superclasses and 179 sub-classes. Figure 9 illustrates the class breakdown of our USC12K dataset.

Object number distribution. Our USC12K dataset contains images with different numbers of objects. For clarify, we have counted the distribution of images with different numbers of objects in USC12K, as shown in the following Table 11.

Table 11. Distribution of Images with Different Numbers of Objects in USC12K.

Number of objects	0	1	2	>2
Number of images	3000	4197	2335	2468

Detail of annotation process. For Scene A and B, we retained their original annotations, while Scene D did not re-

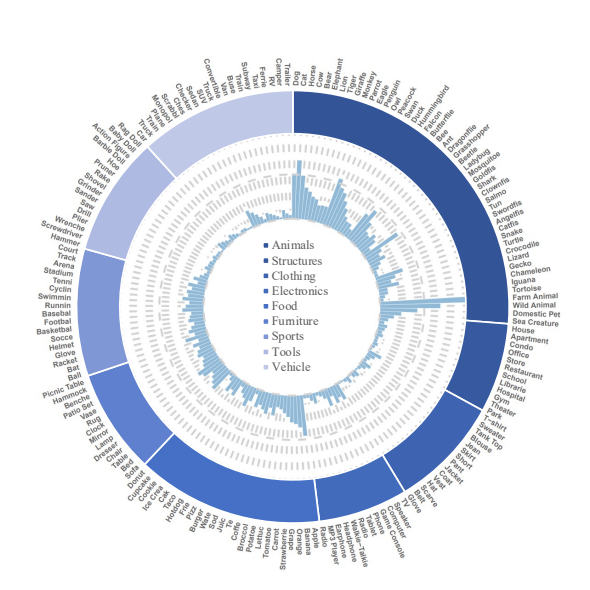


Figure 9. The data source and distribution of different data types.

quire additional annotation. Therefore, we focus here on detailing the annotation process for Scene C.

- Initial Determination of Object Attributes: We invited 7 observers to perform the initial identification of salient and camouflaged objects in the images. A voting process was used to determine the salient and camouflaged objects in each image, with objects and their attributes receiving more than half of the votes being retained. We then used Photoshop to apply red boxes for salient objects and green boxes for camouflaged objects, which served as the reference for the subsequent mask annotation step.
- Mask Annotation: We invited 9 volunteers to perform detailed mask annotation for the dataset using the ISAT interactive annotation tool [21], which supports SAM semi-automatic labeling.
- Annotation Quality Control: After annotation, we invited an additional 3 observers to review and refine the results. Masks with imprecise or incorrect annotations were manually corrected.

More USC12K examples. In Figure 10, we illustrate a selection of images from the USC12K dataset, each featuring both salient and camouflaged objects. The main difference between our USC12K dataset and existing SOD and COD datasets is that it includes a curated subset of 3,000 images, each featuring both salient and camouflaged objects. We invest significant time and effort in finding and annotating these images. Our dataset spans an extensive variety of environments, including, but not limited to, terrestrial, aquatic, alpine, sylvan, and urban ecosystems, and encompasses a broad spectrum of categories, such as lion, flower and various fruit species. This dataset is designed to assist the SOD and COD research communities in advancing the state-of-the-art in discerning more sophisticated saliency and camouflage patterns.

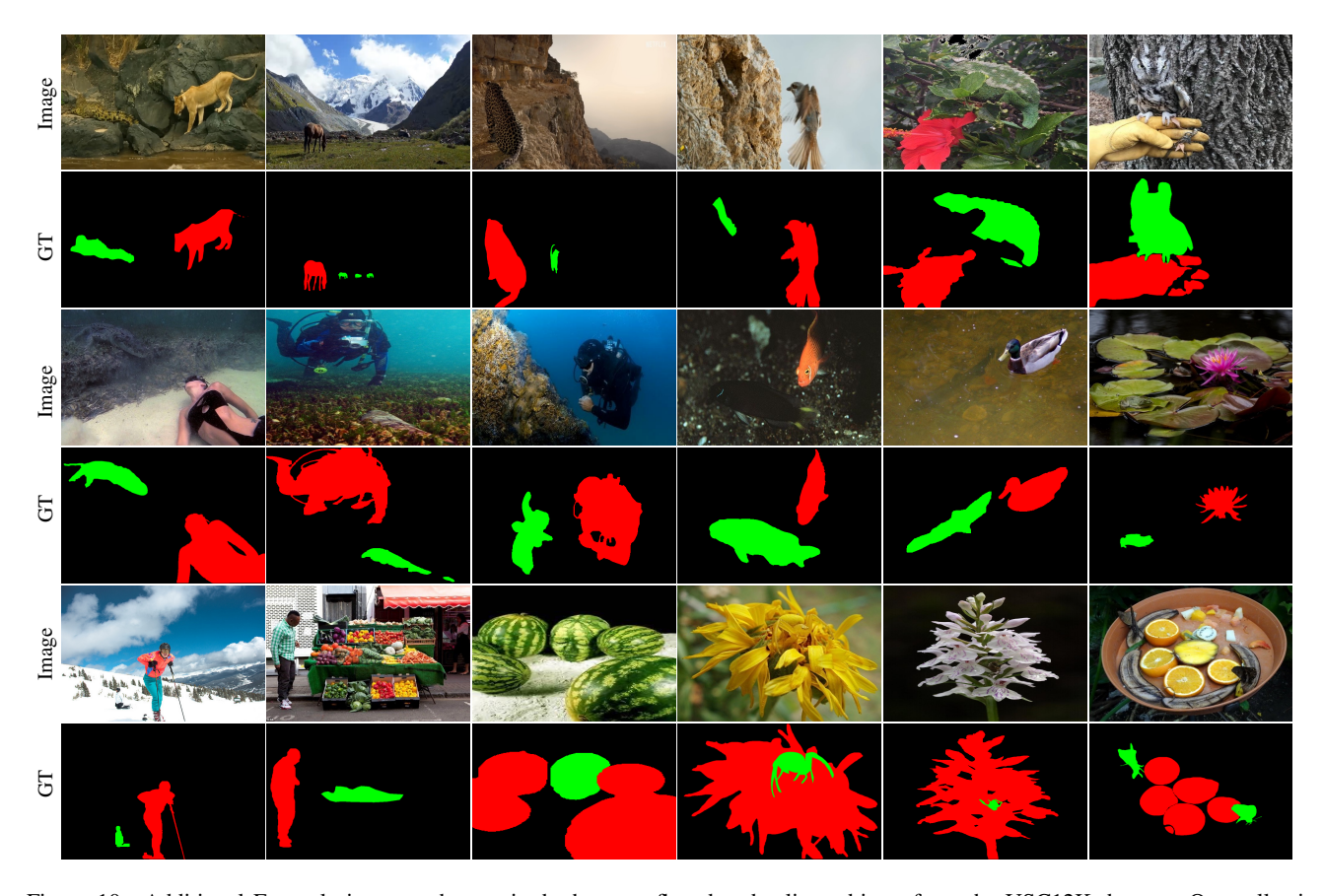


Figure 10. Additional Example images where exist both camouflaged and salient objects from the USC12K dataset. Our collection comprises 3,000 carefully curated and annotated images, encompassing a diverse range of scenes and categories. **Please zoom in for an better view**.

12. Additional Qualitative Results

We present additional predictive results of our USC-Net model compared to other COD and SOD models in the USC12K test set. As illustrated in Figure 11, our model outperforms its competitors. Specifically, across four different scenes, our model demonstrates a high degree of consistency with the ground truth, especially in distinguishing between salient and camouflaged objects. Our model is adept at learning distinctive features of saliency and camouflage. For instance, it can accurately identify patterns such as camouflaged humans (refer to the fifth column of Figure 11). Moreover, in scenes devoid of salient or camouflaged objects, our model remains unaffected by complex backgrounds (refer to the sixth column of Figure 11). This further underscores the robustness and accuracy of our USCNet model.

13. Additional Ablation Study

Performance of Different Base Models. We conducted ablation experiments to evaluate the performance of different base models, as presented in Table 12. First, as shown in the first two and last two rows of the table, our model

Table 12. Performance of different base models. *In the original SAM or SAM2, we only fine-tune the mask decoder.

Method	Base	Para.	IoU_S	IoU_C	mIoU	mAcc	CSCS
SAM*	SAM	3.92	51.07	33.00	59.56	68.73	18.66
USCNet	SAM	4.08	73.93	56.50	75.87	83.86	8.24
SAM2*	SAM2	4.22	66.42	44.02	68.78	77.65	11.58
USCNet	SAM2	4.04	75.57	61.34	78.03	87.92	7.49

demonstrates significant performance improvements on the USC12K benchmark, regardless of whether SAM [23] (default vit-huge version) or SAM2 [54] (default hiera-large version) is used as the base model. For instance, when using SAM as the base model, our method achieves a 16.31% gain in mIoU compared to the original SAM, while utilizing SAM2 results in a 9.25% improvement in mIoU over the original SAM2. Additionally, transitioning from SAM to SAM2 (as shown in rows 2 and 4) results in performance gains across all metrics with fewer fine-tuned parameters.

References

[1] Radhakrishna Achanta, Sheila Hemami, Francisco Estrada, and Sabine Susstrunk. Frequency-tuned salient region de-

- tection. In CVPR, pages 1597–1604, Miami, Florida, USA, 2009. IEEE. 9
- [2] Tianrun Chen, Lanyun Zhu, Chaotao Ding, Runlong Cao, Yan Wang, Shangzhan Zhang, Zejian Li, Lingyun Sun, Ying Zang, and Papa Mao. Sam-adapter: Adapting segment anything in underperformed scenes. In 2023 IEEE/CVF International Conference on Computer Vision Workshops (ICCVW), pages 3359–3367. IEEE, 2023. 3, 5, 7, 11
- [3] Tianrun Chen, Ankang Lu, Lanyun Zhu, Chaotao Ding, Chunan Yu, Deyi Ji, Zejian Li, Lingyun Sun, Papa Mao, and Ying Zang. Sam2-adapter: Evaluating & adapting segment anything 2 in downstream tasks: Camouflage, shadow, medical image segmentation, and more. arXiv preprint arXiv:2408.04579, 2024. 3, 7, 10, 11
- [4] Zhongxi Chen, Ke Sun, and Xianming Lin. Camodiffusion: Camouflaged object detection via conditional diffusion models. In *Proceedings of the AAAI Conference on Artificial Intelligence*, pages 1272–1280, 2024. 7
- [5] Ming-Ming Cheng, Niloy J. Mitra, Xiaolei Huang, Philip H. S. Torr, and Shi-Min Hu. Global contrast based salient region detection. *IEEE TPAMI*, 37(3):569–582, 2015. 4
- [6] Jia Deng, Wei Dong, Richard Socher, Li-Jia Li, Kai Li, and Li Fei-Fei. Imagenet: A large-scale hierarchical image database. In CVPR, pages 248–255, Miami, Florida, USA, 2009. IEEE. 11
- [7] Zijun Deng, Xiaowei Hu, Lei Zhu, Xuemiao Xu, Jing Qin, Guoqiang Han, and Pheng-Ann Heng. R3net: Recurrent residual refinement network for saliency detection. In Proceedings of the 27th international joint conference on artificial intelligence. AAAI Press Menlo Park, CA, USA, 2018.
- [8] Deng-Ping Fan, Ming-Ming Cheng, Yun Liu, Tao Li, and Ali Borji. Structure-measure: A new way to evaluate foreground maps. In *ICCV*, pages 4548–4557, Venice, Italy, 2017. IEEE.
- [9] Deng-Ping Fan, Ming-Ming Cheng, Jiang-Jiang Liu, Shang-Hua Gao, Qibin Hou, and Ali Borji. Salient objects in clutter: Bringing salient object detection to the foreground. In ECCV, 2018. 4
- [10] Deng-Ping Fan, Cheng Gong, Yang Cao, Bo Ren, Ming-Ming Cheng, and Ali Borji. Enhanced-alignment measure for binary foreground map evaluation. In *IJCAI*, pages 1–10, Stockholm, Sweden, 2018. AAAI Press. 9
- [11] Deng-Ping Fan, Ge-Peng Ji, Guolei Sun, Ming-Ming Cheng, Jianbing Shen, and Ling Shao. Camouflaged object detection. In CVPR, pages 2777–2787, 2020. 2, 3, 4, 9, 12
- [12] Deng-Ping Fan, Ge-Peng Ji, Ming-Ming Cheng, and Ling Shao. Concealed object detection. *IEEE TPAMI*, 44(10): 6024–6042, 2021. 1, 2, 3, 6, 7, 9, 10, 11
- [13] Chaowei Fang, Haibin Tian, Dingwen Zhang, Qiang Zhang, Jungong Han, and Junwei Han. Densely nested top-down flows for salient object detection. *Science China Information Sciences*, 65(8):182103, 2022. 3
- [14] Shixuan Gao, Pingping Zhang, Tianyu Yan, and Huchuan Lu. Multi-scale and detail-enhanced segment anything model for salient object detection. *arXiv preprint arXiv:2408.04326*, 2024. 3, 6, 7

- [15] Shang-Hua Gao, Ming-Ming Cheng, Kai Zhao, Xin-Yu Zhang, Ming-Hsuan Yang, and Philip Torr. Res2net: A new multi-scale backbone architecture. *IEEE TPAMI*, 43(2):652–662, 2019. 11
- [16] Chunming He, Kai Li, Yachao Zhang, Longxiang Tang, Yulun Zhang, Zhenhua Guo, and Xiu Li. Camouflaged object detection with feature decomposition and edge reconstruction. In *CVPR*, pages 22046–22055, 2023. 3, 7, 10, 11
- [17] Chunming He, Kai Li, Yachao Zhang, Yulun Zhang, Chenyu You, Zhenhua Guo, Xiu Li, Martin Danelljan, and Fisher Yu. Strategic preys make acute predators: Enhancing camouflaged object detectors by generating camouflaged objects. In *The Twelfth International Conference on Learning Representations*, 2024. 7, 10, 11
- [18] Kaiming He, Xiangyu Zhang, Shaoqing Ren, and Jian Sun. Deep residual learning for image recognition. In CVPR, pages 770–778, Las Vegas, NV, USA, 2016. IEEE. 11
- [19] Qibin Hou, Ming-Ming Cheng, Xiaowei Hu, Ali Borji, Zhuowen Tu, and Philip HS Torr. Deeply supervised salient object detection with short connections. In *Proceedings of the IEEE conference on computer vision and pattern recog*nition, pages 3203–3212, 2017. 3
- [20] Xihang Hu, Xiaoli Zhang, Fasheng Wang, Jing Sun, and Fuming Sun. Efficient camouflaged object detection network based on global localization perception and local guidance refinement. *IEEE Transactions on Circuits and Systems for Video Technology*, 2024. 7, 10, 11
- [21] Shuwei Ji and Hongyuan Zhang. ISAT with Segment Anything: An Interactive Semi-Automatic Annotation Tool, 2023. Updated on 2023-06-03. 12
- [22] Qi Jia, Shuilian Yao, Yu Liu, Xin Fan, Risheng Liu, and Zhongxuan Luo. Segment, magnify and reiterate: Detecting camouflaged objects the hard way. In *Proceedings of* the IEEE/CVF Conference on Computer Vision and Pattern Recognition, pages 4713–4722, 2022. 3
- [23] Alexander Kirillov, Eric Mintun, Nikhila Ravi, Hanzi Mao, Chloe Rolland, Laura Gustafson, Tete Xiao, Spencer Whitehead, Alexander C Berg, Wan-Yen Lo, et al. Segment anything. In *IEEE ICCV*, pages 4015–4026, 2023. 3, 4, 5, 11, 13
- [24] Trung-Nghia Le, Tam V Nguyen, Zhongliang Nie, Minh-Triet Tran, and Akihiro Sugimoto. Anabranch network for camouflaged object segmentation. CVIU, 184:45–56, 2019. 3, 4, 9
- [25] Aixuan Li, Jing Zhang, Yunqiu Lv, Bowen Liu, Tong Zhang, and Yuchao Dai. Uncertainty-aware joint salient object and camouflaged object detection. In CVPR, pages 10071– 10081, 2021. 1, 2, 3
- [26] Feiran Li, Qianqian Xu, Shilong Bao, Zhiyong Yang, Runmin Cong, Xiaochun Cao, and Qingming Huang. Size-invariance matters: Rethinking metrics and losses for imbalanced multi-object salient object detection. In *International Conference on Machine Learning*, pages 28989–29021, PMLR, 2024. 6
- [27] Guanbin Li and Yizhou Yu. Visual saliency based on multiscale deep features. In CVPR, 2015. 3, 4, 9

- [28] Yin Li, Xiaodi Hou, Christof Koch, James M Rehg, and Alan L Yuille. The secrets of salient object segmentation. In CVPR, 2014. 4
- [29] Shijie Lian and Hua Li. Evaluation of segment anything model 2: The role of sam2 in the underwater environment. *arXiv preprint arXiv:2408.02924*, 2024. 3
- [30] Chiuhsiang Joe Lin and Yogi Tri Prasetyo. A metaheuristic-based approach to optimizing color design for military camouflage using particle swarm optimization. *Color Research & Application*, 44(5):740–748, 2019. 1
- [31] Tsung-Yi Lin, Priya Goyal, Ross Girshick, Kaiming He, and Piotr Dollár. Focal loss for dense object detection. In *IEEE ICCV*, pages 2980–2988, 2017. 6
- [32] Weifeng Lin, Ziheng Wu, Jiayu Chen, Jun Huang, and Lianwen Jin. Scale-aware modulation meet transformer. In *Proceedings of the IEEE/CVF International Conference on Computer Vision*, pages 6015–6026, 2023. 11
- [33] Nian Liu and Junwei Han. Dhsnet: Deep hierarchical saliency network for salient object detection. In *Proceedings of the IEEE conference on computer vision and pattern recognition*, pages 678–686, 2016. 3
- [34] Nian Liu, Junwei Han, and Ming-Hsuan Yang. Picanet: Learning pixel-wise contextual attention for saliency detection. In *Proceedings of the IEEE conference on computer* vision and pattern recognition, pages 3089–3098, 2018. 3
- [35] Nian Liu, Ni Zhang, Kaiyuan Wan, Ling Shao, and Junwei Han. Visual saliency transformer. In *ICCV*, pages 4722– 4732, 2021. 3, 6, 7, 10, 11
- [36] Tie Liu, Zejian Yuan, Jian Sun, Jingdong Wang, Nanning Zheng, Xiaoou Tang, and Heung-Yeung Shum. Learning to detect a salient object. *IEEE TPAMI*, 33(2):353–367, 2011.
- [37] Weihuang Liu, Xi Shen, Chi-Man Pun, and Xiaodong Cun. Explicit visual prompting for low-level structure segmentations. In *Proceedings of the IEEE/CVF Conference on Com*puter Vision and Pattern Recognition, pages 19434–19445, 2023. 1, 3, 7, 10, 11
- [38] Ze Liu, Yutong Lin, Yue Cao, Han Hu, Yixuan Wei, Zheng Zhang, Stephen Lin, and Baining Guo. Swin transformer: Hierarchical vision transformer using shifted windows. In *Proceedings of the IEEE/CVF international conference on computer vision*, pages 10012–10022, 2021. 11
- [39] Jonathan Long, Evan Shelhamer, and Trevor Darrell. Fully convolutional networks for semantic segmentation. In CVPR, pages 3431–3440, 2015. 6, 12
- [40] Ange Lou, Yamin Li, Yike Zhang, Robert F Labadie, and Jack Noble. Zero-shot surgical tool segmentation in monocular video using segment anything model 2. arXiv preprint arXiv:2408.01648, 2024. 3
- [41] Ziyang Luo, Nian Liu, Wangbo Zhao, Xuguang Yang, Dingwen Zhang, Deng-Ping Fan, Fahad Khan, and Junwei Han. Vscode: General visual salient and camouflaged object detection with 2d prompt learning. In *Proceedings of the IEEE/CVF Conference on Computer Vision and Pattern Recognition*, pages 17169–17180, 2024. 1, 2, 3, 7, 10, 11
- [42] Yunqiu Lv, Jing Zhang, Yuchao Dai, Aixuan Li, Bowen Liu, Nick Barnes, and Deng-Ping Fan. Simultaneously localize,

- segment and rank the camouflaged objects. In CVPR, pages 11591–11601, 2021. 3, 4, 9
- [43] Jun Ma, Yuting He, Feifei Li, Lin Han, Chenyu You, and Bo Wang. Segment anything in medical images. *Nature Communications*, 15(1):654, 2024. 3
- [44] Ran Margolin, Lihi Zelnik-Manor, and Ayellet Tal. How to evaluate foreground maps? In CVPR, pages 248–255, Columbus, OH, USA, 2014. IEEE. 3, 9
- [45] Haiyang Mei, Ge-Peng Ji, Ziqi Wei, Xin Yang, Xiaopeng Wei, and Deng-Ping Fan. Camouflaged object segmentation with distraction mining. In *CVPR*, pages 8772–8781, 2021. 1, 3, 6, 7, 10, 11
- [46] Vida Movahedi and James H Elder. Design and perceptual validation of performance measures for salient object segmentation. In CVPRW, 2010. 4
- [47] Youwei Pang, Xiaoqi Zhao, Lihe Zhang, and Huchuan Lu. Multi-scale interactive network for salient object detection. In *Proceedings of the IEEE/CVF conference on computer vision and pattern recognition*, pages 9413–9422, 2020. 3
- [48] Youwei Pang, Xiaoqi Zhao, Tian-Zhu Xiang, Lihe Zhang, and Huchuan Lu. Zoom in and out: A mixed-scale triplet network for camouflaged object detection. In CVPR, pages 2160–2170, 2022. 3, 7, 10, 11
- [49] Lintao Peng, Chunli Zhu, and Liheng Bian. U-shape transformer for underwater image enhancement. *IEEE Transactions on Image Processing*, 2023. 4
- [50] Federico Perazzi, Philipp Krähenbühl, Yael Pritch, and Alexander Hornung. Saliency filters: Contrast based filtering for salient region detection. In CVPR, pages 733–740, Providence, RI, USA, 2012. IEEE. 9
- [51] Yongri Piao, Wei Ji, Jingjing Li, Miao Zhang, and Huchuan Lu. Depth-induced multi-scale recurrent attention network for saliency detection. In *Proceedings of the IEEE/CVF* international conference on computer vision, pages 7254– 7263, 2019. 3
- [52] Michael I Posner, Steven E Petersen, et al. The attention system of the human brain. *Annual review of neuroscience*, 13(1):25–42, 1990. 1
- [53] Alec Radford, Jong Wook Kim, Chris Hallacy, Aditya Ramesh, Gabriel Goh, Sandhini Agarwal, Girish Sastry, Amanda Askell, Pamela Mishkin, Jack Clark, et al. Learning transferable visual models from natural language supervision. In *International conference on machine learning*, pages 8748–8763. PMLR, 2021. 4, 12
- [54] Nikhila Ravi, Valentin Gabeur, Yuan-Ting Hu, Ronghang Hu, Chaitanya Ryali, Tengyu Ma, Haitham Khedr, Roman Rädle, Chloe Rolland, Laura Gustafson, et al. Sam 2: Segment anything in images and videos. In *ICLR*, 2025. 3, 11, 13
- [55] Jingjing Ren, Xiaowei Hu, Lei Zhu, Xuemiao Xu, Yangyang Xu, Weiming Wang, Zijun Deng, and Pheng-Ann Heng. Deep texture-aware features for camouflaged object detection. *IEEE Transactions on Circuits and Systems for Video Technology*, 33(3):1157–1167, 2021. 3
- [56] Przemysław Skurowski, Hassan Abdulameer, Jakub Błaszczyk, Tomasz Depta, Adam Kornacki, and Przemysław Kozieł. Animal camouflage analysis: Chameleon database. *Unpublished Manuscript*, 2018. 4

- [57] Martin Stevens and Sami Merilaita. Animal camouflage: current issues and new perspectives. *Philosophical Transactions of the Royal Society B: Biological Sciences*, 364(1516): 423–427, 2009. 1
- [58] Robin Strudel, Ricardo Garcia, Ivan Laptev, and Cordelia Schmid. Segmenter: Transformer for semantic segmentation. In *ICCV*, pages 7262–7272, 2021. 12
- [59] Yujia Sun, Shuo Wang, Chenglizhao Chen, and Tian-Zhu Xiang. Boundary-guided camouflaged object detection. *arXiv* preprint arXiv:2207.00794, 2022. 3
- [60] Longxiang Tang, Kai Li, Chunming He, Yulun Zhang, and Xiu Li. Source-free domain adaptive fundus image segmentation with class-balanced mean teacher. In *International Conference on Medical Image Computing and Computer-Assisted Intervention*, pages 684–694. Springer, 2023. 1
- [61] Laurens Van der Maaten and Geoffrey Hinton. Visualizing data using t-sne. *Journal of machine learning research*, 9 (11), 2008. 8
- [62] Lijun Wang, Huchuan Lu, Yifan Wang, Mengyang Feng, Dong Wang, Baocai Yin, and Xiang Ruan. Learning to detect salient objects with image-level supervision. In CVPR, 2017. 2, 3, 4, 9
- [63] Linzhao Wang, Lijun Wang, Huchuan Lu, Pingping Zhang, and Xiang Ruan. Salient object detection with recurrent fully convolutional networks. *IEEE transactions on pattern anal*ysis and machine intelligence, 41(7):1734–1746, 2018. 3
- [64] Rui Wang, Caijuan Shi, Changyu Duan, Weixiang Gao, Hongli Zhu, Yunchao Wei, and Meiqin Liu. Camouflaged object segmentation with prior via two-stage training. Computer Vision and Image Understanding, 246:104061, 2024. 7, 10, 11
- [65] Tiantian Wang, Ali Borji, Lihe Zhang, Pingping Zhang, and Huchuan Lu. A stagewise refinement model for detecting salient objects in images. In *Proceedings of the IEEE international conference on computer vision*, pages 4019–4028, 2017. 3
- [66] Wenguan Wang, Qiuxia Lai, Huazhu Fu, Jianbing Shen, Haibin Ling, and Ruigang Yang. Salient object detection in the deep learning era: An in-depth survey. *IEEE TPAMI*, 44(6):3239–3259, 2021.
- [67] Wenhai Wang, Enze Xie, Xiang Li, Deng-Ping Fan, Kaitao Song, Ding Liang, Tong Lu, Ping Luo, and Ling Shao. Pvtv2: Improved baselines with pyramid vision transformer. Computational Visual Media, 8(3):1–10, 2022. 11
- [68] Jun Wei, Shuhui Wang, and Qingming Huang. F³ net: fusion, feedback and focus for salient object detection. In *Proceedings of the AAAI conference on artificial intelligence*, pages 12321–12328, 2020. 1, 6, 7, 10, 11
- [69] Yu-Huan Wu, Yun Liu, Le Zhang, Ming-Ming Cheng, and Bo Ren. Edn: Salient object detection via extremely-downsampled network. *IEEE Transactions on Image Processing*, 31:3125–3136, 2022. 6, 7, 10, 11
- [70] Yongqin Xian, Christoph H Lampert, Bernt Schiele, and Zeynep Akata. Zero-shot learning—a comprehensive evaluation of the good, the bad and the ugly. *IEEE TPAMI*, 41 (9):2251–2265, 2018. 4

- [71] Chenxi Xie, Changqun Xia, Mingcan Ma, Zhirui Zhao, Xiaowu Chen, and Jia Li. Pyramid grafting network for one-stage high resolution saliency detection. In *Proceedings of the IEEE/CVF conference on computer vision and pattern recognition*, pages 11717–11726, 2022. 7
- [72] Enze Xie, Wenhai Wang, Zhiding Yu, Anima Anandkumar, Jose M Alvarez, and Ping Luo. Segformer: Simple and efficient design for semantic segmentation with transformers. Advances in neural information processing systems, 34: 12077–12090, 2021. 6, 11
- [73] Yunyang Xiong, Bala Varadarajan, Lemeng Wu, Xiaoyu Xiang, Fanyi Xiao, Chenchen Zhu, Xiaoliang Dai, Dilin Wang, Fei Sun, Forrest Iandola, et al. Efficientsam: Leveraged masked image pretraining for efficient segment anything. arXiv preprint arXiv:2312.00863, 2023. 3
- [74] Qiong Yan, Li Xu, Jianping Shi, and Jiaya Jia. Hierarchical saliency detection. In CVPR, 2013. 4
- [75] Zhiling Yan, Weixiang Sun, Rong Zhou, Zhengqing Yuan, Kai Zhang, Yiwei Li, Tianming Liu, Quanzheng Li, Xiang Li, Lifang He, et al. Biomedical sam 2: Segment anything in biomedical images and videos. arXiv preprint arXiv:2408.03286, 2024. 3
- [76] Chuan Yang, Lihe Zhang, Huchuan Lu, Xiang Ruan, and Ming-Hsuan Yang. Saliency detection via graph-based manifold ranking. In CVPR, 2013. 4, 9
- [77] Fan Yang, Qiang Zhai, Xin Li, Rui Huang, Ao Luo, Hong Cheng, and Deng-Ping Fan. Uncertainty-guided transformer reasoning for camouflaged object detection. In *Proceedings* of the IEEE/CVF international conference on computer vision, pages 4146–4155, 2021. 3
- [78] Bowen Yin, Xuying Zhang, Deng-Ping Fan, Shaohui Jiao, Ming-Ming Cheng, Luc Van Gool, and Qibin Hou. Camoformer: Masked separable attention for camouflaged object detection. *IEEE Transactions on Pattern Analysis and Machine Intelligence*, 2024. 7, 10, 11
- [79] Li Yuan, Yunpeng Chen, Tao Wang, Weihao Yu, Yujun Shi, Zi-Hang Jiang, Francis EH Tay, Jiashi Feng, and Shuicheng Yan. Tokens-to-token vit: Training vision transformers from scratch on imagenet. In *ICCV*, pages 558–567, 2021. 11
- [80] Qiang Zhai, Xin Li, Fan Yang, Chenglizhao Chen, Hong Cheng, and Deng-Ping Fan. Mutual graph learning for camouflaged object detection. In *Proceedings of the IEEE/CVF* conference on computer vision and pattern recognition, pages 12997–13007, 2021. 3
- [81] Wei Zhai, Yang Cao, Jing Zhang, and Zheng-Jun Zha. Exploring figure-ground assignment mechanism in perceptual organization. *Advances in Neural Information Processing Systems*, 35:17030–17042, 2022. 3
- [82] Chaoning Zhang, Dongshen Han, Yu Qiao, Jung Uk Kim, Sung-Ho Bae, Seungkyu Lee, and Choong Seon Hong. Faster segment anything: Towards lightweight sam for mobile applications. arXiv preprint arXiv:2306.14289, 2023.
- [83] Miao Zhang, Tingwei Liu, Yongri Piao, Shunyu Yao, and Huchuan Lu. Auto-msfnet: Search multi-scale fusion network for salient object detection. In *ACM MM*, pages 667–676, 2021. 3, 6, 7, 10, 11

- [84] Miao Zhang, Shuang Xu, Yongri Piao, Dongxiang Shi, Shusen Lin, and Huchuan Lu. Preynet: Preying on camouflaged objects. In *Proceedings of the 30th ACM international conference on multimedia*, pages 5323–5332, 2022. 3
- [85] Xiaoning Zhang, Tiantian Wang, Jinqing Qi, Huchuan Lu, and Gang Wang. Progressive attention guided recurrent network for salient object detection. In *Proceedings of the IEEE conference on computer vision and pattern recognition*, pages 714–722, 2018. 3
- [86] Xiaoqi Zhao, Youwei Pang, Lihe Zhang, Huchuan Lu, and Lei Zhang. Suppress and balance: A simple gated network for salient object detection. In *ECCV*, pages 35–51. Springer, 2020. 3, 6, 7, 10, 11
- [87] Xiaoqi Zhao, Youwei Pang, Wei Ji, Baicheng Sheng, Jiaming Zuo, Lihe Zhang, and Huchuan Lu. Spider: A unified framework for context-dependent concept segmentation. In *ICML*, 2024. 1, 3
- [88] Jiayuan Zhu, Yunli Qi, and Junde Wu. Medical sam 2: Segment medical images as video via segment anything model 2. *arXiv preprint arXiv:2408.00874*, 2024. 3
- [89] Mingchen Zhuge, Deng-Ping Fan, Nian Liu, Dingwen Zhang, Dong Xu, and Ling Shao. Salient object detection via integrity learning. *IEEE TPAMI*, 45(3):3738–3752, 2022. 1, 2, 3, 6, 7, 10, 11



Figure 11. Additional visualizations of the proposed USCNet and other state-of-the-art methods on the USC12K test set. **Zoom-in for better view.**